

Error budgets for the Exoplanet Starshade (Exo-S) Probe-Class Mission study

Stuart B. Shaklan^{1a}, Luis Marchen^a, Eric Cady^a, William Ames^a, P. Douglas Lisman^a, Stefan R. Martin^a, Mark Thomson^a, Martin Regehr^b

^aJet Propulsion Laboratory, California Institute of Technology, 4800 Oak Grove Dr., Pasadena, CA 91109

^bChristie, Parker & Hale, LLP, 655 N. Central Ave. Suite 2300, Glendale, CA 91203

ABSTRACT

Exo-S is a probe-class mission study that includes the Dedicated mission, a 30 m starshade co-launched with a 1.1 m commercial telescope in an Earth-leading deep-space orbit, and the Rendezvous mission, a 34 m starshade intended to work with a 2.4 m telescope in an Earth-Sun L2 orbit. A third design, referred to as the Rendezvous Earth Finder mission, is based on a 40 m starshade and is currently under study. This paper presents error budgets for the detection of Earth-like planets with each of these missions. The budgets include manufacture and deployment tolerances, the allowed thermal fluctuations and dynamic motions, formation flying alignment requirements, surface and edge reflectivity requirements, and the allowed transmission due to micrometeoroid damage.

Keywords: Starshade, occulter, external coronagraph, high contrast imaging

1. INTRODUCTION

We have updated our previous starshade error budget analyses^{1,2} for the Exo-S probe-class missions reported in the Exo-S Science and Technology Definition Team Final Report³, as well as for a slightly larger starshade that has much higher Exo-Earth discovery potential. The starshade error budget determines the manufacturing and deployment tolerances, the allowed thermal fluctuations and dynamic motions, formation flying alignment requirements, surface and edge reflectivity requirements, and the allowed transmission due to micrometeoroid damage.

Error budgets are presented for three probe-class missions. The first is called the “Dedicated” mission because it pairs a 30 m diameter starshade with a 1.1 m telescope whose only purpose is to observe exoplanets when paired with the starshade. The telescope and starshade are launched to an Earth-leading orbit together in a single rocket. The second is called the “Rendezvous” mission. It is a 34 m starshade launched into an L2 orbit where it will join a 2.4 m telescope that does stand-alone science observations in addition to the starshade observations. It was designed as a 2 year technology demonstration mission that also performs science. We refer to the third as the “Rendezvous Earth Finder mission” because it uses a larger, 40 m diameter and a more distant starshade to observe at smaller inner working angles (*i.e.* closer to the target stars) in a 5 year mission. It has roughly 5x higher probability of detecting an Exo-Earth than the Rendezvous technology demonstration mission, and 8x higher probability than the Dedicated mission.

2. MODELING SCATTER IN THE IMAGE PLANE

Shape Tolerancing

Despite starshades falling in the middle of the Fresnel regime, modeling of propagation from starshades turns out to be challenging due to the range of size scales. Edge shapes have tolerances of tens of microns, while the starshade itself is tens of meters across, and the resulting grid sizes required to capture the grid shape details— $10^6 \times 10^6$ or larger—are difficult to propagate with standard Fourier techniques.

Two approaches have emerged to simplify the propagation calculations by reducing the dimensionality of the problem. The first class (Vanderbei et al. 2007⁴) takes advantage of the radial symmetry of the starshade to break the 2D propagation integral into a series of 1D integrals, and the second class (Dubra and Ferrari 1999⁵, Cady 2012⁶) uses line integrals directly around the edge of the starshade to compute the downstream field. Since the second class of algorithms are particularly amenable to modeling changes of edge shape, an implementation of the boundary diffraction wave approach⁶ is used to perform the optical tolerancing for the Exo-S designs.

¹ Email: Stuart.b.shaklan@jpl.nasa.gov; Phone: 818-354-0105

Analysis is performed with electric fields at the focal plane of the appropriate telescope. Perturbations of the starshade orientation or shape are introduced appropriately to capture each error budget term, and the field is computed at the telescope aperture using a line-integral propagator and then at the telescope focal plane using a standard Fourier propagator. A nominal unperturbed field is computed as well. This is repeated for seven wavelengths across the starshade’s usable band, and the entire set of images is fed to the next stage of sensitivity analysis code.

The images are then processed to determine the mean and standard deviation of the radial and azimuthal components of the energy in a circular swath centered at the petal tips. The swath width is determined by ideal telescope point spread function at each wavelength. Sensitivities are computed for local perturbations and are also applied equally to all petals to determine the sensitivity for global perturbations. These sensitivities are imported to a spreadsheet with worksheets set up to track manufacture, deployment, dynamic, thermal, and formation flying error terms.

Modeled Starshade Perturbations

The modeled perturbations mirror the starshade architecture: a spinning central disk supports petals, each of which is made of a lattice truss supporting high-precision 1-m long edge segments and a tip section. Table 1 lists the corresponding perturbations. Broadly speaking, the error budget addresses: petal placement and petal shape inaccuracies; departures of the starshade from its nominal location; and scattering effects from secondary source (besides the target star). These error contributors are a function of manufacturing tolerances, deployment tolerances, dynamics, thermal behavior, formation flying limitations, and starshade edges and surface features. The error budget presented here includes allocations for each of these groups. Figure 1 illustrates one term in the error budget, segment displacement normal to the petal axis, and the corresponding change in image plane contrast.

The perturbations fall into seven distinct categories:

Random (local) perturbations are unique to a petal or a location on a petal, e.g., radial displacement of a petal, or a cyclical shape error on one of the petal segments. It is assumed that uncorrelated random perturbations exist over the whole starshade. Image plane intensity increases as the square of the perturbation amplitude, and intensities from independent perturbations add linearly.

Bias (global) perturbations are common to all petals or petal structures (e.g., radial displacement of all petals by the same amount, or a common cyclical shape error that appears on segment number 3 of all petals). These types of errors may arise from biases in metrology during assembly, systematic machining errors during manufacture, and a number of other causes such as systematic differences between the assembled structure on the ground and its post-deployment shape in space.

Truss perturbations are related to defects in the truss and are analyzed with a set of circular harmonics (e.g., elliptical deformation) and truss dynamic modes. Analysis of harmonics higher than the elliptical mode is incomplete at this time.

Residual thermal perturbations are the imprint of shadowing on the rotating starshade; petals cool down as they pass through the shadow of the spacecraft, then warm up as they reappear in the sunlight. The petal thermal response function leaves a warming circular footprint around the starshade.

Formation flying and starshade attitude perturbations lead to scatter in the image plane from both lateral and longitudinal formation flying errors, and starshade orientation.

Table 1. Modeled starshade error budget terms.

Manufacture/ Deployment	Description
Petal Position	Radial, lateral, in-plane clocking, rotation about spine
Segment Shape	0.5, 1, 2, 3, 4, cycle sine and cosine
Segment Placement	Tangential, normal, in-plane clocking
Tip Segment Placement	Radial, azimuthal, in-plane clocking
Truss Ellipticity	In-plane elliptical deformation
Petal Shape + Tip Clip	In-plane and out-of-plane bending, broken tip
Thermal	Description
Uniform Petal Expansion	Petal multiplicative shape change
Uniform Truss Expansion	Radially displaces petals
Radial Gradient	Petal base to tip gradient (length and width)
Harmonic Gradient	1, 2, 3, 4, 5 cycles/petal (width only)
Formation Flying	Description
Lateral Displacement	Decentration of telescope from center of shadow
Longitudinal Displacement	Position of telescope along line-of-sight to starshade
Other	Description
Solar Glint	Sunlight glinting off of petal edges
Surface Scatter	Earthshine, etc. scattering from telescope-facing surface
Holes	Starlight leakage from micrometeoroids

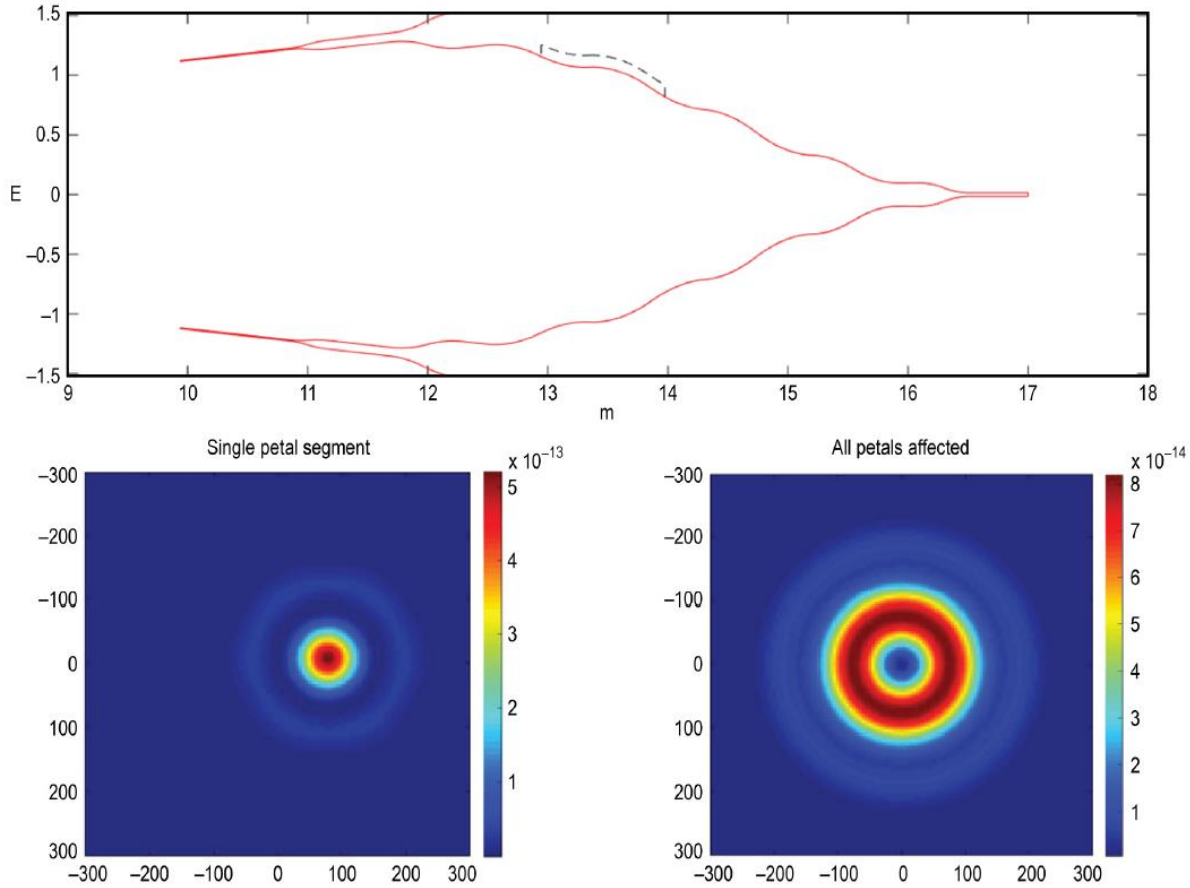


Figure 1. Example of local petal perturbation; a 1-m long petal segment is displaced normal to the petal axis. The perturbation is shown enlarged 1000x relative to the displacement in the tolerancing axis. Axes in the image plane are milli-arcseconds. Colors are image plane contrast. Left: single petal perturbation. Right: the same perturbation is applied to all petals.

Holes in the starshade allow starlight to leak directly to the telescope. Some of this light will be coherent with the other perturbations, while multiply-scattered light will add incoherently. Holes also allow sunlight to enter and escape the starshade.

Glint and reflection scatter light from the Sun or other astronomical bodies (e.g., the Earth, Jupiter, the Milky Way) into the telescope.

The first six categories are linked directly to the target star and contributions are expressed in terms of contrast (the ratio of scatter to the peak of the image of the star when it is not blocked by the starshade). The last category, glint and reflection, as well as solar leakage through holes, contributes to the background but is independent of the brightness of the target star. Thus, the contrast contribution is a function of the star's brightness relative to the scatter source.

It is important to keep in mind that the starshade is spinning at 1/3 rpm and that this is much shorter than the integration time to observe planets. Local perturbations are smeared into full circular arcs and, like global perturbations, they do not contribute to background 'speckles'. The arcs contribute photometric (Poisson) noise, but do not present a systematic noise floor. Likewise, scatter from holes and from random formation flying errors does not lead to a systematic noise floor as these are averaged by spinning and by time, respectively.

However, the starshade is not immune to systematic speckles. Residual thermal perturbations are present and cause an asymmetry linked to the spacecraft shadow. Biases in formation flying also lead to asymmetric scatter. Finally solar glint

leaves a distinct two-lobe pattern in the direction toward the Sun, while the conical cover of the central disk leads to a non-symmetric scatter component from bright astronomical bodies.

3. ALLOCATIONS

Photometric Requirements

Error budget tolerances are allocated to meet a top-level contrast requirement while remaining consistent with tolerances achieved in the starshade technology development program. The contrast requirement has two parts: photometric and systematic. The photometric requirement ensures that the instrument scatter level is below the scatter due to zodiacal and exozodiacal light. We conservatively assume a total zodiacal flux that is seven times the nominal 23 mag/sq arcsec of the local zodi. With this background, an instrument contrast of 1×10^{-10} with the Rendezvous Mission increases the background counts and the integration time by $\sim 15\%$ for a $V=5$ star and 37% for a $V=4$ star. For brighter stars, the instrument background is still more important, but integration times become so short that overall impact on performance is minimal.

The Dedicated Mission collects roughly 1/5 as much target light as the Rendezvous Mission, and the same amount of zodiacal light (per pixel). Thus, an instrument contrast of 5×10^{-10} has the same impact on integration time as 1×10^{-10} does for the Rendezvous Mission and is adopted as the photometric floor for the Dedicated Mission.

Systematic Requirements

The systematic requirement is much more stringent than the photometric floor. The starshade is designed to observe exoplanets as deep as 4×10^{-11} times fainter than the target star ($\Delta\text{mag} = 26$). The systematic requirement adopted here is to keep the local speckle contrast at this level and to calibrate the contrast as required for planet detection. Thus for an SNR of 10 relative to the systematic noise level, calibration by a factor of 10 to 4×10^{-12} is required. Top level requirements are summarized in Table 2.

Table 2. Starshade contrast requirements

Requirement	Dedicated 1.1 m	Rendezvous 2.4 m
Photometric Floor	5×10^{-10}	1×10^{-10}
Systematic Floor	4×10^{-11}	4×10^{-11}

Key Tolerances

The contrast requirements are met by allocating key tolerances in accordance with the results of the starshade technology program, briefly summarized here. A full-scale petal that met the shape requirements for exo-Earth detection was developed in TDEM-09.⁷ High-precision (but not razor-blade sharp) optical edges were attached with a precision of 15 μm rms (about $\pm 45 \mu\text{m}$ tolerance). The segment shapes were measured to be within 30–45 μm tolerance in low spatial frequencies, and 15 μm tolerance in high spatial frequencies. The overall petal shape was accurate to $\pm 100 \mu\text{m}$.

A representative inner disk structure, 12 m in diameter, was tested for petal deployment precision in TDEM-10.⁸ Petals were attached with a global tolerance within $\pm 100 \mu\text{m}$ of their ideal design point. Multiple deployments showed that the petal positions repeated to a tolerance of $\pm 200 \mu\text{m}$.

In addition to these technology results, dynamics modeling of the disk structure and thermal modeling of petal transients show that these terms will not be significant contributors to the error budget. Thruster firings for station keeping will induce several microns of petal motion and these will damp out to a negligible one micron level after about 10 s. Petals spend about 5 seconds passing through the shadow of the spacecraft as the starshade rotates at 1/3 rpm. Thermal modeling shows that petal width changes are below 1 μm and can be neglected.

Table 3 lists the key tolerances that drive the photometric and systematic floors. The single most critical parameter in both the Dedicated and Rendezvous mission designs is the global radial placement of the petals. This term is especially significant in the Dedicated Mission design and is allocated the bulk of the pre-launch error budget as shown in Figure 2. The allocation for petal radial position is 150 μm in the Dedicated Mission design and 200 μm for the Rendezvous Mission design—a relaxation compared to the 100 μm achieved in TDEM-10. Additionally, 100 μm (Dedicated) and 250 μm (Rendezvous) is allocated for petal radial post-launch position changes that were not captured in the TDEM tests.

The overall temperature of the starshade, and the difference in temperature between the central disk and petals, are also critical. The allowed strain difference between the truss and petals is 20 ppm (Dedicated Mission) and 40 ppm

Table 3. Allocated starshade tolerances.

	Dedicated 1.1 m	Contrast × 10 ⁻¹¹	Rendezvous 2.4 m	Contrast × 10 ⁻¹¹
Manufacture				
Petal Segment Shape (Bias)	14 μm	1.4	22 μm	0.37
Petal Segment Shape (Random)	71 μm	0.5	71 μm	0.26
Petal Segment Placement (Bias)	4 μm	0.7	7 μm	0.07
Petal Segment Placement (Random)	45 μm	0.6	53 μm	0.47
Pre-Launch Deployment				
Petal Radial Position (Bias)	150 μm	6.0	200 μm	0.15
Petal Radial Position (Random)	450 μm	0.6	450 μm	0.1
Post-Launch Deployment				
Petal Radial Position (Bias)	100 μm	2.7	250 μm	0.23
Petal Radial Position (Random)	350 μm	0.4	375 μm	0.06
Thermal				
Disk-Petal Differential Strain (Bias)	20 ppm	6.0	40 ppm	0.6
1-5 Cycle/Petal Width (Bias)	10 ppm	1.0	30 ppm	0.2
Formation Flying				
Lateral Displacement	1 m	2.9	1 m	1.1
Longitudinal Displacement	250 km	2.5	250 km	0.43

(Rendezvous Mission). Thermal models discussed in the Exo-S report³ show that these strain differences are achieved over a range of incident solar angles from 30–83° from the starshade normal.

The other driving terms in the error budget are the segment shape and segment placement tolerances. The segment shape tolerance (±71 μm) is ~50% larger than the tolerance achieved in TDEM-09. Margin was added to account for potential difficulties in manufacturing a sharp edge with the correct shape over a 1-m segment. The segment placement requirement of 45 μm (for the Dedicated Mission) was achieved in TDEM-09. The Rendezvous Mission design allows a 50% relaxation of the segment placement requirement. Table 4 compares TDEM achievements with Exo-S requirements.

Table 4. Key requirements and achieved performance.

Key Technology	Demonstration	Achieved Tolerance	Required Tolerance
Petal Segment Shape (Random)	TDEM-09	±45 μm	±68 μm
Petal Segment Position (Random)	TDEM-09	±45 μm	±45 μm
Radial Petal Position (Bias)	TDEM-10	±100 μm	±150 μm

The longest wavelength of the bandpass is most sensitive to perturbations, and the Dedicated mission design is more sensitive than the Rendezvous Mission design. Figure 2 shows the manufacturing error budgets for the shortest and longest bands of both the Dedicated and Rendezvous missions. The contrast values for the allocated manufacturing tolerances are listed above the pie charts. The larger value for the Dedicated mission design shows that it almost 6 times more sensitive to perturbations at the long wavelength limit than the Rendezvous mission design. This is mainly due to the lower spatial resolution of the telescope spreading scattered energy out to the IWA.

Overall Performance and Performance Reserve

The high-level, 90% confidence error starshade photometric error budgets, exclusive of holes, edge glint, and surface reflectivity, are shown in Figure 3. The manufacturing budgets, constituting about 20% of the total, have already been discussed. The thermal budgets constitute ~25% of the total. For the Dedicated Mission design, this is driven by differential strain between the petals and the truss over a range of solar angles. Formation flying accounts for 11% and 16% of the photometric budgets in the Dedicated and Rendezvous mission systems, respectively. The ‘nominal’ term in the error budget pie charts refers to the limiting performance of the ideal starshade.

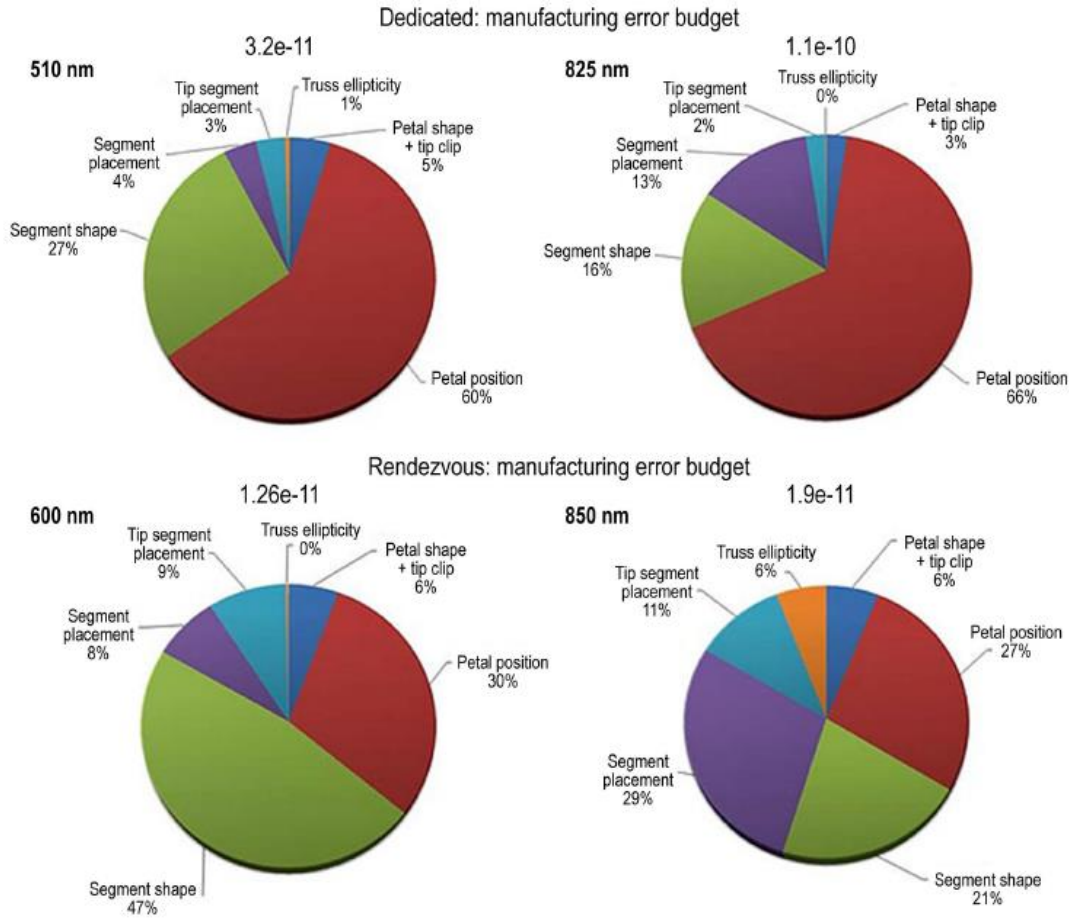


Figure 2. Pre-launch manufacturing error budget.

The systematic noise floor is driven by lateral formation flying bias. A bias of 0.4 m contributes to an rms level of 1.7×10^{-11} (Dedicated) and 5×10^{-12} (Rendezvous). The starlight leaking around the starshade is not circularly symmetric in the image plane and can masquerade as a planet. This level of systematic error will require a modest calibration factor of ~ 4 for SNR=10 detection of $\Delta mag=26$ exoplanets for the Dedicated Mission design, and achieves SNR=8 without calibration for the Rendezvous Mission design.

As noted earlier, dynamics models show that a few seconds after a thruster firing (which happens every few hundred seconds), vibrations dampen to a micron level, at which petal motions can be neglected. The dynamics requirements for in plane petal motion are 50 μm and 50 microradians, and out-of-plane rotations are even less restricted. Thus, dynamics is expected to be an insignificant contributor to starshade performance.

The error budgets in this pre-phase A study do not include model uncertainty factors. However, both designs carry 50% performance reserve (equivalent to 33% of the total error budget). This reserve

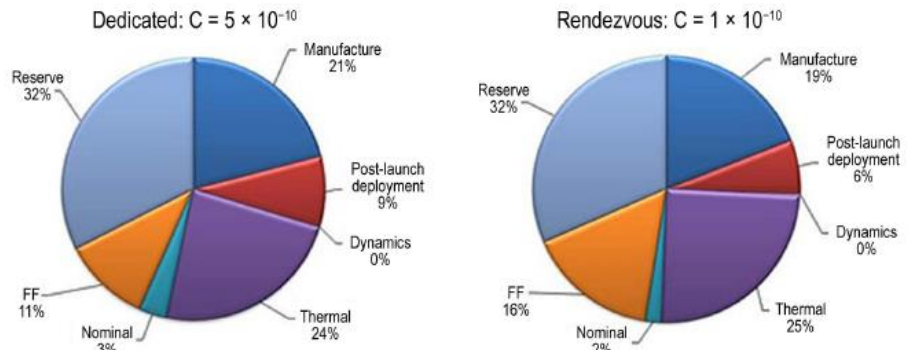


Figure 3. Overall error budget at long wavelength limit.

posture is reasonable because:

- The largest contributors to the error budget have already been demonstrated on hardware with flight-like materials and structures;
- Dynamics and thermal gradient models show a large performance margin;
- Performance degradation with loss of contrast is gradual;
- Only a moderate level of calibration is needed; and
- The systematic error related to formation flying is a function of three parameters (lateral offset, azimuth of the offset, and longitudinal offset) making its calibration relatively simple.

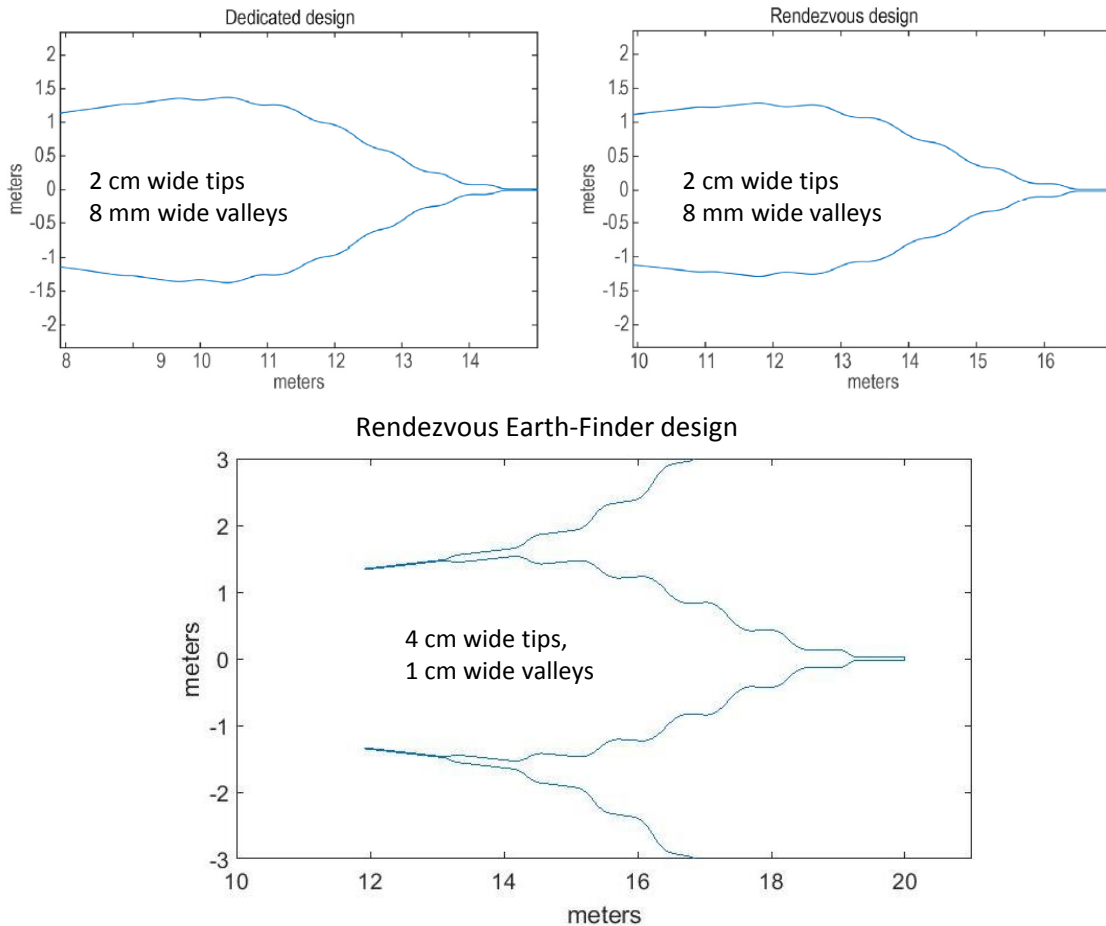


Figure 4. Comparison of petal shapes for the Dedicated, Rendezvous, and Rendezvous Earth Finder designs. Note that parts of adjacent petals are shown in the Earth Finder panel.

Requirements for Rendezvous Earth Finder

The Rendezvous Earth Finder mission employs a 40 m diameter starshade consisting of a 24 m diameter truss and 8 m long petals. The petals are depicted in Figure 4 in comparison to the smaller Dedicated and Rendezvous designs. The starshade is designed to work with an IWA of ~ 50 mas in a bandpass spanning 400-540 nm. The starshade design derives from an ongoing trade study addressing observing approaches that maximize the observational completeness of habitable zones subject to constraints on launchable fuel mass (limited by launch vehicle capacity), starshade slew acceleration (limited by the number and type of engines), fractional on-sky integration time (to allow the telescope to do other science), and instrument limitations such as the systematic noise floor and throughput. An important part of the trade study is to find the optimal balance between the IWA and observing bandwidth. Cady (2011⁹) showed that by

narrowing the spectral bandwidth, increases integration times due to loss of photons. The IWA can be reduced by moving the star away from the telescope while still maintaining exquisite starlight rejection. Smaller apertures improve access to the HZ, but the increased telescope/starshade separation increases the time between targets. Initial results of this are reported in Seager,¹⁰ and Trabert.¹¹

Detailed modeling of the Rendezvous Earth Finder mission shows that its tolerancing is similar to the Rendezvous mission except for a few key parameters identified in Table 5. Both obtain 10-10 contrast, but the tighter IWA of the Rendezvous Earth Finder (50 mas vs. 100 mas for Rendezvous), which is only partially offset by the shorter wavelength band (maximum wavelength 540 nm vs. 850 nm for Rendezvous), drives the petal positioning, thermal strain, and tip segment strain to values 20-50% smaller than in the Rendezvous mission. The tolerances are nonetheless still within the values achieved by the TDEM-10 work and our modeling results.

Sensitivity to petal edge ripples

We note that the edge ripples of the Rendezvous Earth Finder petals are larger than in the Exo-S designs. The ripples appeared because we relaxed the smoothness constraint on the edges to achieve the deepest possible nominal shadow depth. The question arises as to whether the edge ripples increase the sensitivity to petal motion and impact engineering requirements, as has been predicted in the literature.¹² Here we show that the petal positioning tolerance is highly insensitive to the size of the ripples.

Figure 5 shows three designs for the Rendezvous Earth Finder. All three designs have a 24 m inner disk and 8 m long petals with ~4 cm wide tips and 1cm wide gaps at the petal bases. The top one, designated LN15, is the baseline design. It achieves the best overall nominal contrast across the band, as shown in Table 6. The table shows that the ripples mainly control the contrast at the red end of the bandpass.

Radial motion of the petals (i.e. the petals shown in Figure 5 are displaced to the right or left relative to the inner disk) scatters light. We show in Table 7 that the rippled petal LN15 is indeed slightly more sensitive to motion at the red end of the bandpass, though it is actually less sensitive to motion at the blue end. Overall the three petal designs have nearly identical sensitivity to motion, even though the ripple amplitude in LN15 is several times larger than in LU21 and LU7. The difference in sensitivities has an insignificant impact on engineering requirements. The rippled design is slightly preferred because of its superior nominal performance, though all three designs are acceptable.

Table 5. Key tolerances in Rendezvous and Earth Finder

	Rendezvous	Earth Finder
Pre-Launch Deployment		
Petal Radial Position (Bias)	200 um	200 um
Post-Launch Deployment		
Petal Radial Position (Bias)	250 um	200 um
Thermal		
Disk-Petal Differential Strain (Bias)	20 ppm	13 ppm
Tip segment strain	500 ppm	250 ppm

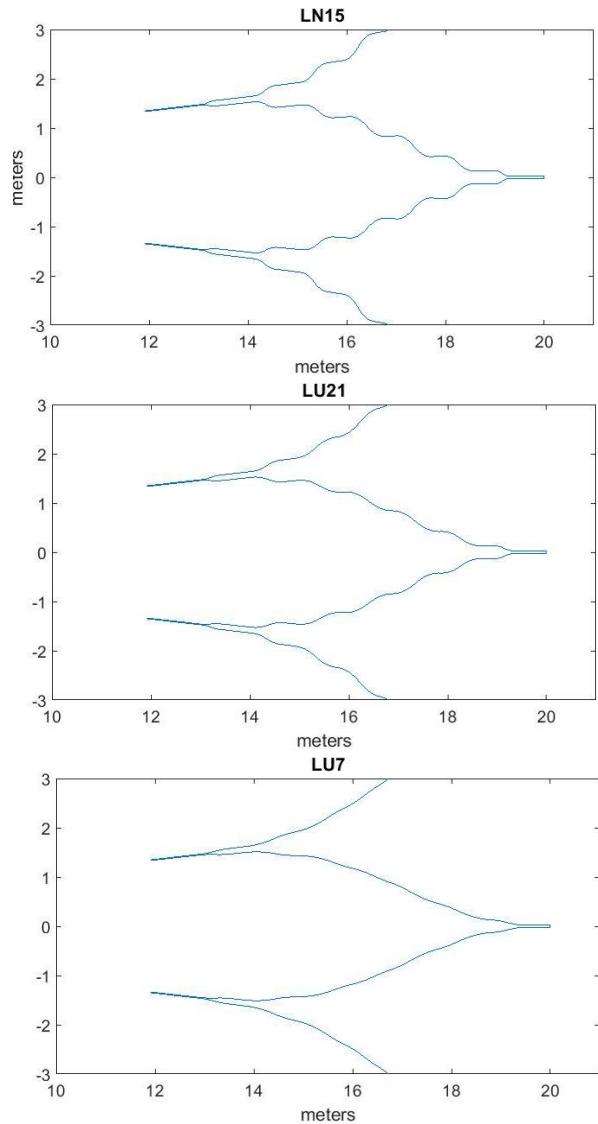


Figure 5. LN15 is the Rendezvous Earth Finder design. LU21 and LU7 are designations for designs with 8 m long petals and an increasing smoothness constraint.

is slightly preferred because of its superior nominal

Table 6. Nominal contrast for petals of increasing smoothness

Nominal Contrast * 1e-12			
	400 nm	475 nm	550 nm
LN15	3.8	2.3	6.9
LU21	3.7	2.3	7.6
LU7	3.9	2.1	9.3

Table 7. Change in contrast for petals of increasing smoothness

Sensitivity to 0.5 mm radial petal motion

Δ Contrast * 1e-12			
	400 nm	475 nm	550 nm
LN15	8.5	12.5	10.1
LU21	8.7	12.3	8.9
LU7	8.8	12.1	6.2

Starshade uses two layers with cm-scale spacing, likely a foam panel, between layers. If a micrometeoroid were to puncture all layers, the result would be a series of pinholes illuminated by other pinholes. Even if all the holes were aligned toward the telescope, the multiple scatter reduces the transmitted field strength at each layer, and also scrambles the phase of the final transmitted field. This cancels the leakage fields at the telescope more effectively than direct transmission distributed across the starshade. Thus, the tolerances here are conservative, and can probably be relaxed after further analysis. Modeling of the integrated micrometeoroid flux shows that even for a single layer blanket, the $\leq 1 \text{ cm}^2$ hole area allocation is satisfied.¹³ However, this does not account for seasonal micrometeoroid showers when the flux increases by up to two orders of magnitude. A couple of times a year it will be necessary to turn the starshade edge-on to the shower for a period of 1 or 2 weeks.

Solar Leakage

Sunlight shines on the back of the starshade. Material transmission and micrometeoroid holes allow the light to enter the back and escape through the front. Some of this light will be captured by the telescope. We model the sunlight passing through by treating the optical shield as two identical layers of Kapton each separated by a small gap from the interior foam spacer, as illustrated in Figure 6. In the physical shield the foam serves as a spacer between the Kapton layers. While it is extensively light-weighted, there will still be regions where the foam connects to the Kapton. We ignore these for simplicity. Holes in the Kapton and foam are assumed to be small relative to the total area of holes, numerous, and evenly distributed. We also assume the two layers of Kapton have the same reflectivity and hole fraction. This is reasonable as the micrometeoroid population is generally isotropic.

The power transmitted by a surface is treated as equal to the power incident on the surface multiplied by this hole fraction, plus a term representing light transmitted directly through the material. When light enters a closed region of the shade, the beam is treated as reflecting off both surfaces an infinite number of times, with a certain amount of light transmitted through to the far side and a certain amount absorbed on each reflection. This allows us to determine the amount of incident light exiting the shade on the telescope side. The telescope side of the optical shield is then treated as a Lambertian light source to determine the amount of sunlight arriving at the telescope.

Mathematically we treat the starshade optical shield like an optical cavity, computing the fraction of incident light that exits relative to the light that enters after accounting for the steady-state levels of light reflecting and absorbing the

4. HOLES AND OPACITY

Leakage

The optical shield consists of two layers of black Kapton with a spacer material, e.g. open cell foam. Conservatively at some fraction of the starlight passes through these layers. If the shield is slightly perturbed, the overall opacity requirement is to restrict the amount of light leaking through at a level of better than 10^{-11} . Thus each layer requires an opacity of $\sim 10^{-6}$. Testing of the Kapton shows that the material is sufficiently opaque. In reality, any light passing through the starshade will encounter the central foam layer, and while passing through the Kapton the wavefronts will be perturbed; both effects will greatly reduce the scatter and further relax the single-layer opacity requirement.

The starshade will be bombarded by micrometeoroids while in space. A cumulative pinhole area of 1 cm^2 is allocated for leakage of starlight through holes created by micrometeoroids and the associated contrast allocation is found to be 1×10^{-12} . This analysis assumed each pinhole is like an ideal aperture in a single-layer thin screen. However, the

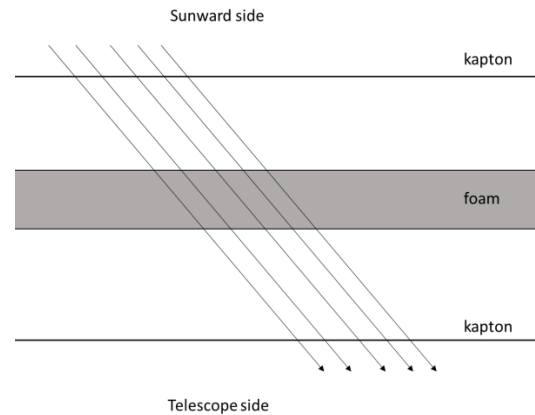


Figure 6. Starshade optical shield model for solar leakage calculations.

internal layers shown in Figure 6. We treat all reflections internal to the cavity as specular, creating a ‘baths’ of light between the Kapton and foam layers. The Kapton hole fraction, ranging from 0 (no holes) to 1 (completely holes: no Kapton remaining) is labeled as H_K , its transmittance is labeled t_K and its reflectance is labeled r_K . The total fraction of incident light reflected off a Kapton surface will be labeled R_K , and expressed as $R_K = r_K(1-H_K)$. Similarly, the fraction of incident light passing through a Kapton surface, T_K , is $T_K = t_K(1-H_K) + H_K$. Similar expressions can be written in terms of the foam reflectance r_f , transmittance t_f , and hole fraction H_f .

Given some irradiance I_{in} shining on the back side of the starshade, we find that the light escaping the optical shield on the telescope side due to all possible paths entirely within the lower gap (no reflections, two reflections, 4 reflections, etc.):

$$I_{out} = \frac{T_K^2 T_F}{(1 - R_F R_K)^2 - R_K^2 T_F^2} I_0$$

We now calculate how much of this light reaches the telescope. With an irradiance of I_{out} from the entire surface of Starshade, the optical power emitted by the shade $P_{out} = I_{out} A_{shade}$, where A_{shade} is the area of the optical shield. If we treat the optical shield as a Lambertian source radiating into a hemisphere, with a telescope of aperture area $A_{telescope}$ a distance r away from the shade, the power collected by the telescope is

$$P_{telescope} = \frac{A_{telescope}}{\pi D^2} P_{out}$$

We use these equations to derive the allowed hole area such that the starshade appears to be no brighter than 1/10 the flux of the faintest targets to be observed by the starshade. These are planets that are 26 magnitudes fainter (4×10^{-11}) than their 6th magnitude stars, or $V=32$ mag. Notably this is 59 magnitudes fainter than the Sun itself!

We show the allowed hole area as a function of foam transmittance in Figure 7, for the worst case scenario of the sun just 30° off the starshade normal. The plot assumes Kapton reflectivity, $r_K = 0.5$, foam transmittance $r_f = 0.1$, opaque Kapton, and small hole fraction. As long as the foam transmittance is below 10%, the starshade will appear fainter than $V=34.5$ with tens of square cm of holes on each side. This requirement is conservative with respect to other sources of starshade illumination such as edge glint and front-side illumination by astronomical targets.

5. SOLAR GLINT FROM STARSHADE EDGES

A small fraction of incident sunlight reflects and diffracts from the starshade optical edge into the telescope to appear as solar glint and contributes to instrument background noise. Specular reflection and solar diffraction is limited to portions of the edge that are oriented normal to the Sun–starshade–telescope plane, as shown in Figure 8. Diffuse reflections may originate from any illuminated part of the starshade edge, but tend to be stronger where the specularly reflected light originates.

Glint Predictions and Measurements

A starshade system model was developed to predict solar glint fluxes as a function of solar incidence angle. The model was validated by testing a variety of representative edges in a scatterometer testbed, developed for this purpose.¹⁴

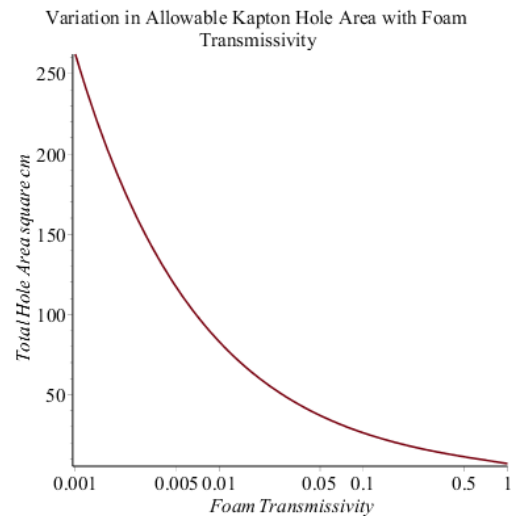


Figure 7. Permissible hole area vs. foam transmittance. The integrated starshade magnitude is 34.5. We assume that the kapton reflectivity is $r_k=0.5$ and the foam reflectivity is $r_f = 0.1$.

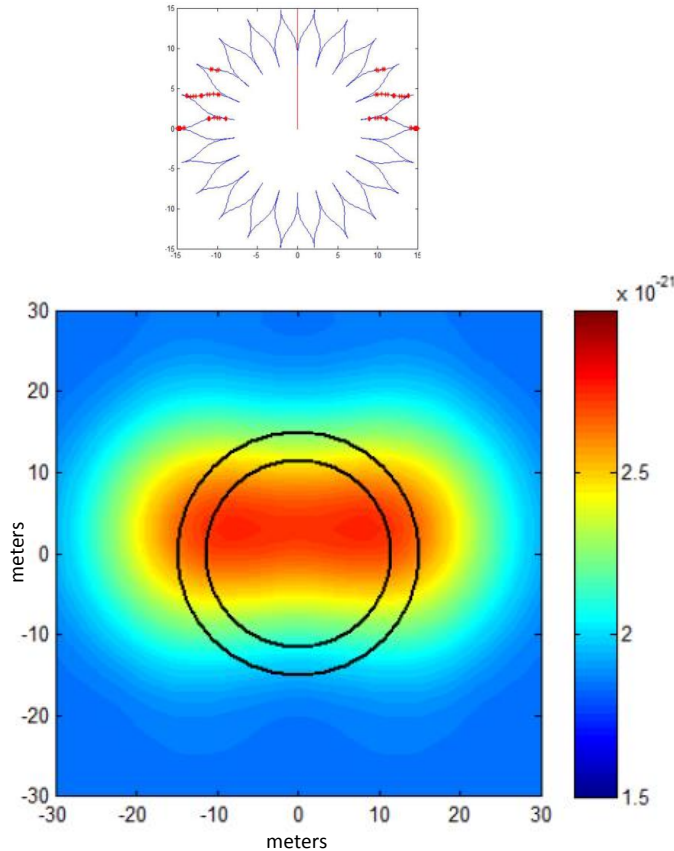


Figure 8. Top: The Sun is above and behind the starshade. Horizontal edges diffract and specularly reflect sunlight towards the telescope. Bottom: on the same spatial scale, the scatter is shown for S polarization against the Zodiacal background. The resolution limit corresponds to the Dedicated mission's 1.1 m aperture in the visible.

the two glinting areas producing the dog-bone shape of the region shown in yellow. The lobe brightness is equivalent to a point source at 27 visual magnitudes and

Optical Edge Scatter

Fundamentally, the scatter is limited by diffraction even when the edge is infinitely sharp. The diffraction term is equivalent to a source of magnitude $V = 27-28$ (depending on the solar angle to the starshade surface) near the end of the petal. The allocated post-calibration contrast is 1×10^{-11} and this translates to the following edge engineering specification:

Product of edge radius of curvature (μm) \times reflectivity (%) ≤ 12

This edge engineering specification ensures that light scattered by reflection is well below the level of diffraction. The diffracted light in turn is below the assumed level of exozodiacal and zodiacal light ($V = 21$ per sq arcsec in the Exo-S study). Calibration of edge scatter is straightforward because the scatter is

Figure 9 compares model predictions to measurements of a commercial stainless steel razor blade for the Dedicated mission. The model is in excellent agreement with measurements over solar incidence angles between about 50° and 80° . Diffracted sunlight is the dominant term and the sum of all reflected sunlight is at least 1 visual magnitude dimmer than diffracted light.

The tested razor blade is representative of a physical limit and is not intended as a flight solution since its geometry is not ideal. It accurately represents the diffraction, which is independent of edge radius of curvature (RoC) and reflectivity (R). The reflected flux for other edge designs can be scaled in proportion to the product of RoC and R (i.e., edge surface area). The tested razor blade had a $0.2\text{-}\mu\text{m}$ RoC and was highly specular with 60% reflectivity. Any similarly specular edge with a $\text{RoC} \times R$ product of 12 will reflect the same solar flux into the telescope.

Solar glint affects image plane background illumination at 60° solar incidence (Figure 8). A high performance specular edge like the razor blade is assumed. The rectangular area corresponds to a region of the sky around the star, shown as a $60\text{ m} \times 60\text{ m}$ area at the starshade plane. The outer circle represents the extreme extent of the starshade (the location of the tips). The general background produced by exozodiacal light (blue color on figure) is amended by the glint, which is seen as two lobes arising from the edge locations where diffraction and specular reflection occur. For Exo-S, diffraction limited imaging results in smoothing and blurring together of

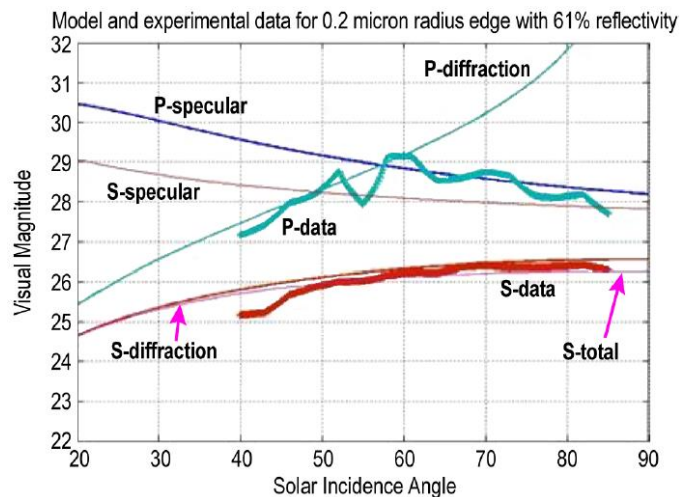


Figure 9. Model and experimental data for a razor blade.

a function of a single parameter (solar angle), the starshade spins so that only the average edge shape matters, and the scatter level will be nearly constant during the mission.

In addition to the edge radius requirement, the optical edge must accommodate bending strain, associated with petal stowing, and thermal strain, associated with any mismatch in material CTE relative to the petal structure.

None of these requirements are individually difficult to achieve. In combination, however, they present a moderate material design challenge.

6. REFLECTIVITY OF THE STARSHADE

Because the starshade reflectivity is less than unity, it will appear, on average, darker than the surrounding heavens. But occasionally, a bright source such as Jupiter or the center of the Milky Way appears behind the telescope and reflects from the starshade into the telescope aperture. Here we model the reflectivity and compute the apparent magnitude of the starshade for worst-case illuminations.

The starshade has a central disk covered by a truncated cone, and a number of flat petals around its perimeter. The normal to the surface of the cone is 6° from the axis of the starshade at all points on the cone. This telescope-facing side is covered in black, rip-stop Kapton, installed so that the grid of reinforcing rip-stop threads faces away from the telescope. The material has a relatively, but not perfectly, matte finish and a surface texture with waves resulting from the presence of the fibers on the reverse side of the material.

When a point on the starshade is illuminated by a source of light, such as Jupiter, the amount of light reflected from a region around the point into the telescope depends on the angle between the incident light and the local normal to the surface of the starshade, and the angle between the local normal and the direction to the telescope. The Kapton surface of the starshade is modeled using a combination of measurement and interpolation, and the reflectivity of the starshade is calculated using numerical integration over the flat and conical areas of the starshade.

The BRDF Model

The bidirectional reflectance distribution function (BRDF) of the Kapton was measured by Surface Optics Corporation of San Diego, California, for five incident zenith angles: 0° , 20° , 40° , 60° , and 80° . For each incident zenith angle, the BRDF was measured for various reflected zenith and azimuth angles, with finer spacing near the specular direction for the non-zero zenith angle.

A net reflectivity curve is computed after integrating the BRDF numerically over the conical portion of the surface of the starshade, and adding the contribution from the flat portions of the starshade. When light is incident at 40° from the starshade normal, the reflectivity is about 1%, a reduction of 5 magnitudes of the incident light level. It continues to drop at larger angles.

Figure 10 shows the appearance of the starshade when illuminated by a light source 12° from normal. Most of the reflected energy appears to come from the region of the cone, and is removed by >1 petal length (7 m, or 40 mas) from the IWA defined by the petal tips. The scattered light affects only a portion of the image plane, and only partially overlaps the innermost planets to be observed.

Illumination by Astronomical Bodies

Table 8 shows the results of the worst-case illumination by the brightest astronomical sources: Venus, Jupiter, and Mars; and the central region of the Milky Way. Illumination by Venus is less of an issue than Jupiter or Mars because solar pointing restrictions ensure that Venus at its brightest is no closer than 53° from the starshade normal.

Illumination by Earthshine

The minimum allowed illumination for Earthshine is computed for heliocentric Earth-leading, Earth drift-away and L2 orbits. Using the Pallé et al. (2003) model¹⁴ of the Earth's albedo, it is determined that to keep the starshade apparent magnitude fainter than 30, at a distance of 0.1 AU the Earth should be no closer than 81° to the starshade normal, while

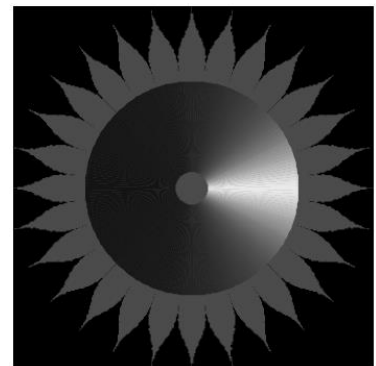


Figure 10. Starshade as it would appear when illuminated by an off-axis point source.

Table 8. Apparent Magnitude of Starshade

Source	Worst-Case Apparent Magnitude of Starshade
Jupiter	29.7
Mars	29.7
Venus	31.3
Milky Way	29.6

at 0.2 AU it should be no less than 60° from normal. For a wide L2 Lissajous orbit, the non-Lambertian component of the albedo brightens the limb of the Earth and restricts all Earthshine from the front of the starshade, which may place target-dependent seasonal pointing restriction on the starshade in its periodic L2 orbit unless alternative approaches are pursued. These Earthshine illumination results apply to the baseline black Kapton material. An alternative approach is to select a highly specular material

and design the cover to minimize slopes due to ripples. This makes the system practically immune to illumination by off-axis sources, effectively removing Earth-pointing restrictions. However, the specular surface would be susceptible to bright glints from sources behind the telescope. This alternative approach is currently under study.

7. DICHROIC FILTER REJECTION REQUIREMENTS

The starshade is designed to operate over a finite optical band at a specific distance. When the distance is changed, the starshade continues to form a dark shadow for an optical band that is shifted in inverse proportion to the distance. This allows one to trade IWA, which grows (making planets more difficult) as the starshade moves closer (reducing fuel consumption and time to move between targets) and the band grows redder (which is advantageous for characterization). For the Rendezvous mission, we take advantage of the finite bandpass to utilize the WFIRST/AFTA coronagraph direct imaging camera and IFS for both imaging and guiding functions. When the starshade is more distant, the blue band (Figure 11) is used. The dark hole is formed between 400 and 600 nm, and the bright light leaking above 600 nm is used for guiding. The light level remains below 1/1000 of the star’s flux out to 1 um, where the detector quantum efficiency drops. In the region near 900 nm a suppression of $\sim 10^{-7}$ is required. When the starshade is moved closer for NIR characterization, the red band is used. The shadow approaches a level of 10^{-2} near the Ag-coated optics cutoff below 400 nm. In this region, the dichroic filters must provide an attenuation of 10^{-8} in the imaging channel while directing the blue guide light to the guiding channel. This suppression can be achieved with a single or with multiple filters – the challenge is to maintain high throughput while suppressing out-of-band light.

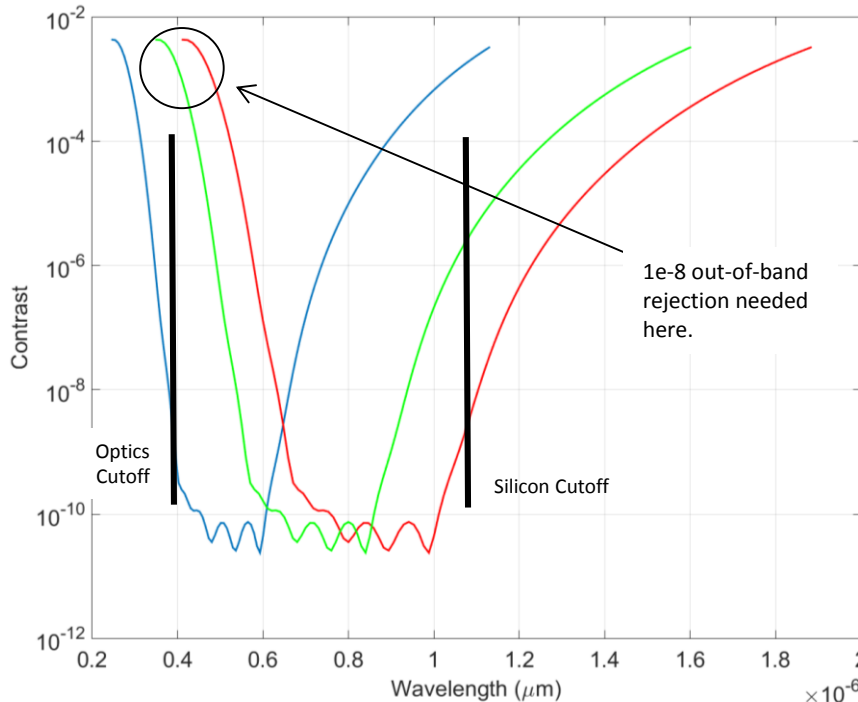


Figure 11. Bandpass for the Rendezvous mission for three different starshade-telescope distances. When positioned for observation in the red and guiding in the blue (red curve), rejection of 1e-8 is required below ~500 nm.

8. CONCLUSIONS

The Exo-S Dedicated and Rendezvous missions and the Rendezvous Earth Finder mission present challenges that are well understood and within the bounds of proven technology. A vigorous technology plan is in place to bring the required starshade technologies to TRL-5 within the next few years. The plan builds upon past successful TDEM work, including demonstration of a petal built to the accuracy required for Exo-Earth detection, and inner disk deployment proven to the same criterion, as well as imaging demonstrations to levels approaching 10^{-9} contrast in 2-km long tests on a dry lakebed.¹⁵ Currently four TDEM activities are funded, including: (jointly) lab tests at Princeton at the flight Fresnel number (approximately 12) with a goal of 10^{-9} suppression and 10^{-10} contrast, co-funded with development of a full flight-like petal; optical edge materials and scattering demonstration (at NGAS); formation flying sensing and control demonstration, to be carried out on the Princeton testbed; and a recently selected development, build and demonstration of an optical shield on a half-scale testbed (JPL/NGAS). Additional modeling and infrastructure is funded through the Exoplanet Exploration program and internal studies at JPL. This supports a scatterometer¹⁶ facility for optical edge testing as well as facilities in support of the half-scale testbed.

This work was carried out at the Jet Propulsion Laboratory, California Institute of Technology, under contract to the National Aeronautics and Space Administration.

REFERENCES

- [1] Shaklan, S. B., *et al.*, “Error budgeting and tolerancing of starshades for exoplanet detection,” Proc. SPIE 7731, 77312G (2010).
- [2] Shaklan, S. B., *et al.*, “A starshade petal error budget for exo-earth detection and characterization,” Proc. SPIE 8151, 815113 (2011).
- [3] Seager, S., *et al.*, “Exo-S: starshade probe-class exoplanet direct imaging mission concept Final Report,” http://exep.jpl.nasa.gov/stdt/Exo-S_Starshade_Probe_Class_Final_Report_150312_URS250118.pdf (2015).
- [4] Vanderbei, R. J. *et al.*, “Optimal occulter design for finding extrasolar planets,” ApJ, 665, 794 (2007).
- [5] Dubra, A., and Ferrari, J. A., “Diffracted field by an arbitrary aperture,” Am. J. Phys, 67, 87-92 (1999).
- [6] Cady, E., “Boundary diffraction wave integrals for diffraction modeling of external occulter,” Opt. Express, 20 15196 (2012).
- [7] Kasdin, N. J., *et al.*, “Technology demonstration of starshade manufacturing for NASA’s Exoplanet Mission Program,” Proc. SPIE 8442, 84420A (2012).
- [8] Webb, D., *et al.*, “Successful starshade petal deployment tolerance verification in support of NASA’s technology development for exoplanet missions,” Proc. SPIE 9151, 91511P (2014).
- [9] Cady, E., “Nondimensional representations for occulter design and performance evaluation,” Proc. SPIE 8151, 815112 (2011).
- [10] Seager, S., *et al.*, “The Exo-S Probe Class Starshade Mission,” Proc. SPIE 9605 (this conference, 2015).
- [11] Trabert, R., *et al.*, “Design reference mission for the Exoplanet Starshade (Exo-S) Probe-Class study,” Proc. SPIE 9605 (this conference, 2015).
- [12] Cash, W., “Analytical Modeling of Starshades,” ApJ 738, 76 (2011).
- [13] Arenberg, J. Glassman, T., and Lo, A., “Effects of scattered light on the performance of the New Worlds Starshade,” Proc. SPIE 6693, 66931E (2007).
- [14] Pallé *et al.*, “Earthshine and the Earth’s albedo: 2. Observations and simulations over 3 years,” J. Geophys. Res., 108(D22), 4170 (2003).
- [15] Glassman, T., *et al.*, “Measurements of high-contrast starshade performance,” Proc. SPIE 9143, 91432O (2014).
- [16] Martin, S., *et al.*, “Starshade optical edge modeling, requirements, and laboratory tests,” Proc. SPIE 8864, 88641A (2013).